The Astrophysical Journal, 807:167 (9pp), 2015 July 10 doi:10.1088/0004-637X/807/2/167

NuSTAR AND MULTIFREQUENCY STUDY OF THE TWO HIGH-REDSHIFT BLAZARS S5 0836+710 AND PKS 2149–306

G. Tagliaferri[1], G. Ghisellini[1], M. Perri[2,3], M. Hayashida[4], M. Baloković[5], S. Covino[1], P. Giommi[2], G. M. Madejski[6], S. Puccetti[2,3], T. Sbarrato[1,7], S. E. Boggs[8], J. Chiang[6], F. E. Christensen[9], W. W. Craig[9,10], C. J. Hailey[11], F. A. Harrison[5], D. Stern[12], and W. W. Zhang[13]

[1] INAF—Osservatorio Astronomico di Brera, via E. Bianchi 46, I-23807 Merate, Italy; gianpiero.tagliaferri@brera.inaf.it
[2] ASI—Science Data Center, via del Politecnico, I-00133 Rome, Italy
[3] INAF—Osservatorio Astronomico di Roma, via Frascati 33, I-00040 Monteporzio Catone, Italy
[4] Institute for Cosmic Ray Research, University of Tokyo, 5-1-5 Kashiwanoha, Kashiwa, Chiba, 277-8582, Japan
[5] Cahill Center for Astrophysics, California Institute of Technology, 1200 East California Boulevard, Pasadena, CA 91125, USA
[6] Kavli Institute for Particle Astrophysics and Cosmology, SLAC National Accelerator Laboratory, Menlo Park, CA 94025, USA
[7] Dipartimento di Fisica G. Occhialini, Università di Milano Bicocca, Piazza della Scienza 3, I-20126 Milano, Italy
[8] Space Sciences Laboratory, University of California, Berkeley, CA 94720, USA
[9] DTU Space—National Space Institute, Technical University of Denmark, Elektrovej 327, DK-2800 Lyngby, Denmark
[10] Lawrence Livermore National Laboratory, Livermore, CA 94550, USA
[11] Columbia Astrophysics Laboratory, Columbia University, New York, NY 10027, USA
[12] Jet Propulsion Laboratory, California Institute of Technology, Pasadena, CA 91109, USA
[13] NASA Goddard Space Flight Center, Greenbelt, MD 20771, USA
Received 2015 March 4; accepted 2015 May 18; published 2015 July 9

ABSTRACT

Powerful blazars are flat-spectrum radio quasars whose emission is dominated by a Compton component peaking between a few hundred keV and a few hundred MeV. We observed two bright blazars, PKS 2149–306 at redshift $z = 2.345$ and S5 0836+710 at $z = 2.172$, in the hard X-ray band with the *Nuclear Spectroscopic Telescope Array* satellite. Simultaneous soft-X-rays and UV–optical observations were performed with the *Swift* satellite, while near-infrared (near-IR) data were obtained with the Rapid Eye Mount telescope. To study their variability, we repeated these observations for both sources on a timescale of a few months. While no fast variability was detected during a single observation, both sources were variable in the X-ray band, up to 50%, between the two observations, with larger variability at higher energies. No variability was detected in the optical/NIR band. These data, together with *Fermi*-Large Area Telescope, *Wide-field Infrared Survey Explorer*, and other literature data, are then used to study the overall spectral energy distributions (SEDs) of these blazars. Although the jet nonthermal emission dominates the SED, it leaves the UV band unhidden, allowing us to detect the thermal emission of the disk and to estimate the black hole mass. The nonthermal emission is well reproduced by a one-zone leptonic model by the synchrotron, self-Compton, and external Compton processes. Our data are better reproduced if we assume that the location of the dissipation region of the jet, $R_{\rm diss}$, is in between the torus and the broad-line region. The observed variability is explained by changing a minimum number of model parameters by a very small amount.

Key words: BL Lacertae objects: individual (PKS 2149–306, S5 0836+710) – galaxies: active – galaxies: jets – quasars: general – X-rays: general

1. INTRODUCTION

Blazars are a subclass of active galactic nuclei whose emission is dominated by a relativistic jet pointing toward us. Their emission extends from the radio band to the γ-ray and TeV band and is dominated by nonthermal processes. Their spectral energy distribution (SED) is dominated by two humps. The first, spanning the infrared to the X-ray band, is usually attributed to synchrotron emission, while the second, located from the X-ray to the γ-ray band, is attributed to the inverse Compton scattering process. This second component can be produced by energetic electrons scattering only their own synchrotron photons (synchrotron self-Compton, SSC for short), or also scattering radiation produced externally to the jet (i.e., external Compton, EC for short). The latter process is likely to be important especially in those sources for which the second component is largely dominating the SED. This usually occurs for flat-spectrum radio quasars (FSRQs), which are among the most luminous persistent sources of the universe. As such, they can be detected in almost all bands also at high redshifts, well above $z > 5$ (Romani et al. 2004; Sbarrato et al. 2012).

The most powerful FSRQs are therefore very bright hard X-ray and γ-ray sources, with the hard X-ray band (20–150 keV) more effective in selecting bright FSRQs at $z > 4$ (Ajello et al. 2009; Ghisellini et al. 2010a), while the γ-ray band (0.1–10 GeV) is very effective up to z= 2–3 (Ghisellini et al. 2011; Giommi et al. 2013; Shaw et al. 2013). Hard X-ray and γ-ray surveys recently obtained with the Burst Alert Telescope (BAT, on board the *Swift* satellite; Gehrels et al. 2004) and the Large Area Telescope (LAT, on board *Fermi*; Atwood et al. 2009) instruments (Ajello et al. 2009, 2014; Cusumano et al. 2010; Nolan et al. 2012) provide us the opportunity to see whether the jet properties evolve with cosmic time (Ghisellini et al. 2011; 2013; Volonteri et al. 2011). Moreover, the nonthermal SED of these powerful sources leaves the UV band unhidden (the synchrotron hump peaks at much smaller frequencies, and the high-energy hump at much larger energies; Sbarrato et al. 2013), and at these frequencies the thermal accretion flux can emerge and be

detected. This allows us to study the relation between the jet power and the accretion luminosity.

It is clear from the above that the hard X-ray and γ-ray bands are crucial to characterize the properties of these sources. In particular, the hard X-ray band (10–100 keV) is where the Compton component is rapidly rising, but it is also the band in which up to now we did not have very sensitive instruments (e.g., compared to those at softer X-rays). Thanks to the advent of the *Nuclear Spectroscopic Telescope Array* (*NuSTAR*) satellite (Harrison et al. 2013), it is now possible to obtain detailed X-ray spectra in the 3–79 keV band for moderately bright X-ray sources. Therefore, we selected two bright blazars, PKS 2149–306 at redshift $z = 2.345$ and S5 0836+710 at $z = 2.172$, and organized simultaneous observing campaigns - with the *NuSTAR* and *Swift* satellites, plus on-ground optical/near-infrared (NIR) observations for PKS 2149–306. Both are detected in the γ-ray band by *Fermi*-LAT.

Both sources are high-redshift, bright blazars with an SED dominated by the Compton component. PKS 2149–306 was detected up to 100 keV with the PDS detector on board the *BeppoSAX* satellite with a very flat hard X-ray spectrum (energy spectral energy index $\alpha \simeq 0.4$; Elvis et al. 2000). A flat hard X-ray spectrum up to 100 keV was later also detected with *INTEGRAL* (Bianchin et al. 2009) and *Swift*/BAT (Sambruna et al. 2007). This source is detected in the γ-ray band by the *Fermi*-LAT detector (Nolan et al. 2012). S5 0836 +710 has been detected up to 100 keV with the PDS detector on board the *BeppoSAX* satellite with a very flat hard X-ray spectrum (energy index $\alpha \simeq 0.4$, Tavecchio et al. 2000). The source has also been detected both by *INTEGRAL* (Beckmann et al. 2006) and *Swift*/BAT (Sambruna et al. 2007). In particular, the BAT detection shows a steeper spectrum, $\alpha \simeq 0.8$, and a flux a factor of ∼5 weaker than the one recorded with *BeppoSAX* (Sambruna et al. 2007). This blazar is a bright and variable γ-ray source already detected by the Energetic Gamma-ray Experiment Telescope (onboard the *Compton Gamma Ray Observatory*; Hartman et al. 1999), with flare activity recently seen with the *Fermi*-LAT detector (Akyuz et al. 2013).

Here we present the results of simultaneous observations obtained in the X-ray band with *NuSTAR* and with the X-ray Telescope (XRT; Burrows et al. 2005) on board *Swift* for the two blazars. For both sources we repeated these observations over a timescale of a few months to check for source variability. The X-ray data are complemented with simultaneous optical/UV data taken with the Ultraviolet/Optical Telescope (UVOT; Roming et al. 2005) on board *Swift* and, for PKS 2149–306, with optical/NIR data from the robotic Rapid Eye Mount (REM) telescope (Zerbi et al. 2004) located in La Silla, Chile. For both sources we also analyze the *Fermi*-LAT data over a 1 yr timescale centered on our *NuSTAR* and *Swift* observations. While we were in the process of submitting this work, a paper appeared on astro-ph presenting these data of S5 0836+710 (Paliya 2015). That paper is more concentrated on the γ-ray variability, but it also analyzes and discusses the SED of this source. We will briefly compare our results with the one of that paper in the discussion.

In this work, we adopt a flat cosmology with $H_0 = 70$ km s^{-1} Mpc^{-1} and $\Omega_M = 0.3$.

2. OBSERVATIONS AND DATA ANALYSIS

The *NuSTAR* and *Swift* (and for PKS 2149–306, also REM) observations are integrated with data from the *Wide-field Infrared Survey Explorer* (*WISE*[14]) satellite (Wright et al. 2010) and with archival data from the NASA/IPAC Extragalactic Database (NED) and the ASI Science Data Center (ASDC).

2.1. NuSTAR Observations

The *NuSTAR* satellite carries two co-aligned hard XRTs, each consisting of a mirror module focusing high-energy X-ray photons in the band 3–79 keV onto two independent shielded focal plane modules (FPMs), referred to here as FPMA and FPMB (Harrison et al. 2013).

The *NuSTAR* satellite observed PKS 2149–306 on 2013 December 17 (obsID 60001099002) and on 2014 April 18 (obsID 60001099004). The total net exposure times were 38.5 and 44.1 ks, respectively. S5 0836+710 was observed by *NuSTAR* on 2013 December 15 (obsID 60002045002) and on 2014 January 18 (obsID 60002045004), for total net exposure times of 29.7 and 36.4 ks, respectively.

The FPMA and FPMB data sets were first processed with the NuSTARDAS software package (v.1.4.1) jointly developed by the ASDC (Italy) and the California Institute of Technology (Caltech, USA). Event files were calibrated and cleaned with standard filtering criteria with the *nupipeline* task using version 20140414 of the *NuSTAR* CALDB.

For all four observations the FPMA and FPMB spectra of the sources were extracted from the cleaned event files using a circle of 20 pixel (∼49″) radius, while the background was extracted from two distinct nearby circular regions of 50 pixel radius. The ancillary response files were generated with the *numkarf* task, applying corrections for the point-spread function (PSF) losses, exposure maps, and vignetting. All spectra were binned to ensure a minimum of 20 counts per bin. Both sources are quite bright and well detected by *NuSTAR* up to 79 keV.

2.2. Swift Observations

Swift (Gehrels et al. 2004) observed PKS 2149–306 on 2013 December 16–17 (obsIDs 00031404013 and 00031404014) and on 2014 April 18 (obsID 00031404014), and S5 0836+710 was observed on 2013 December 16 (obsIDs 00080399001) and on 2014 January 18 (obsID 00080399002).

2.2.1. XRT Observations

The XRT on board *Swift* is sensitive to the 0.3–10 keV X-ray energy band (Burrows et al. 2005). All XRT observations were carried out using the most sensitive Photon Counting readout mode. The XRT data sets were first processed with the XRTDAS software package (v.3.0.0) developed at the ASDC and distributed by HEASARC within the HEASoft package (v. 6.16). Event files were calibrated and cleaned with standard filtering criteria with the *xrtpipeline* task using the calibration files available in version 20140709 of the *Swift*-XRT CALDB.

The two individual XRT event files for the 2013 December observations of PKS 2149–306 were merged together using the XSELECT package for a total net exposure time of 8.0 ks. The

[14] Data retrieved from the *WISE* All-sky Source Catalog: http://irsa.ipac.caltech.edu/.

Table 1
UVOT Vega *v*, *b*, *u*, *W*1, *M*2, *W*2 Observed Magnitudes of PKS 2149–306 and S5 0836+710 (Magnitudes Not Corrected for Galactic Extinction)

Date	*v*	*b*	*u*	*W*1	*M*2	*W*2
			PKS 2149–306			
2013 Dec 17	17.83 ± 0.11	17.86 ± 0.06	17.14 ± 0.06	18.22 ± 0.10	20.46 ± 0.07	…
2014 Apr 18	17.61 ± 0.05	17.75 ± 0.02	17.14 ± 0.02	18.06 ± 0.04	20.00 ± 0.11	20.12 ± 0.08
			S5 0836+710			
2013 Dec 15	…	…	…	…	17.45 ± 0.03	…
2014 Jan 18	16.95 ± 0.03	17.12 ± 0.02	16.22 ± 0.02	16.92 ± 0.03	17.53 ± 0.04	17.91 ± 0.03

Table 2
REM AB (*gri*) and VEGA (*JHK*) Observed Magnitudes of PKS 2149–306 (Magnitudes Not Corrected for Galactic Extinction)

Date	*g*	*r*	*i*	*J*	*H*	K_s
2013 Dec 15	17.82 ± 0.05	17.58 ± 0.06	17.40 ± 0.06	16.56 ± 0.06	16.00 ± 0.08	15.10 ± 0.11
2013 Dec 19	17.75 ± 0.05	17.36 ± 0.06	17.38 ± 0.06	16.58 ± 0.07	15.89 ± 0.07	15.22 ± 0.13

net exposure time of the 2014 April observation was 6.4 ks. For the two observations of S5 0836+710 the total net exposure times were 1.9 and 4.7 ks, respectively. For all observations the energy spectra were extracted from the summed cleaned event files. Events for the spectral analysis were selected within a circle of 20 pixel (∼47″) radius, which encloses about 90% of the PSF, centered on the source position. The background was extracted from a nearby circular region of 50 pixel radius. The ancillary response files were generated with the *xrtmkarf* task, applying corrections for the PSF losses and CCD defects using the cumulative exposure map. The source spectra were binned to ensure a minimum of 20 counts per bin.

2.2.2. UVOT Observations

UVOT observations were performed with all six optical and UV lenticular filters (namely, *W*2, *M*2, *W*1, *u*, *b*, *v*; Roming et al. 2005). We performed aperture photometry for all filters in all observations using the standard UVOT software distributed within the HEAsoft package (version 6.15.1) and the calibration included in the latest release of the CALDB. Counts were extracted from an aperture of 5″ radius for all filters and converted to fluxes using the standard zero points (Poole et al. 2008). The fluxes were then de-reddened using the appropriate values of $E(B-V)$ taken from Schlegel et al. (1998) and Schlafly et al. (2011) with $A_\lambda/E(B-V)$ ratios calculated for UVOT filters using the mean Galactic interstellar extinction curve from Fitzpatrick & Massa (1999). These fluxes were then used to build the SEDs of both sources (see Figure 5). No variability was detected within single exposures in any filter. The processing results were carefully verified checking for possible contamination from nearby objects within the source apertures and from objects falling within background apertures. Both sources are well detected in all filters. The values of the magnitudes in the Vega system are given in Table 1.

2.3. REM Observations

We observed PKS 2149–306 with the REM (Zerbi et al. 2004), a robotic telescope located at La Silla Observatory (Chile). It performed photometric observations in the optical *gri* and NIR *JHK* filters in the nights of 2013 December 15 and 19. REM has a Ritchey–Chretien configuration with a 60 cm *f*/2.2 primary and an overall *f*/8 focal ratio in a fast-moving alt-azimuth mount that provides two stable Nasmyth focal stations. The two cameras, REMIR (Conconi et al. 2004) for the NIR and ROS2 (Molinari et al. 2014) for the optical, both have the same field of view of 10′ × 10′. The telescope is able to operate in a fully autonomous way (Covino et al. 2004), and data are reduced and analyzed following standard procedures. Aperture photometry was derived by means of custom tools,[15] and calibration was based on objects in the field of view reported in the APASS[16] and 2MASS[17] catalogs in the optical and NIR, respectively.

Table 2 reports the observed *gri* (AB) and *JHK* (Vega) photometry measured on the two nights, not corrected for the Galactic extinction of $E(B-V)=0.02$ from Schlegel et al. (1998).

2.4. Fermi-*LAT* Observations

Both sources are also bright γ-ray emitters and are regularly detected by *Fermi*-LAT. We analyzed the data collected for 1 yr between 2013 June 01 and 2014 June 01 (MJD 56,444–56,809) following the standard procedure,[18] using the *Fermi*-LAT analysis software `ScienceTools v9r34p1` with the `P7REP_SOURCE_V15` instrument response functions. Events in the energy range 100 MeV–300 GeV were extracted within a 15° acceptance cone of the Region of Interest (ROI) centered on the location of each source. Gamma-ray fluxes and spectra were determined by an unbinned maximum likelihood fit with `gtlike`. The background model included all known γ-ray sources within the ROI from the second *Fermi*-LAT catalog (Nolan et al. 2012).[19] Additionally, the model included the isotropic and Galactic diffuse emission components. Flux normalization for the diffuse and background sources were left free in the fitting procedure.

The *Fermi*-LAT light curves above 100 MeV binned over a timescale of 7 days are shown in Figure 1 for both sources. We mark with vertical dotted lines the dates of the *NuSTAR*

[15] https://pypi.python.org/pypi/SRPAstro.FITS/
[16] http://www.aavso.org/apass
[17] http://www.ipac.caltech.edu/2mass/
[18] http://fermi.gsfc.nasa.gov/ssc/data/analysis/
[19] In order to test the effect of possible new gamma-ray sources not included in 2FGL, we reanalyzed the data using the *Fermi*-LAT 4 yr point source catalog (3FGL; Acero et al. 2015), finding fully consistent results.

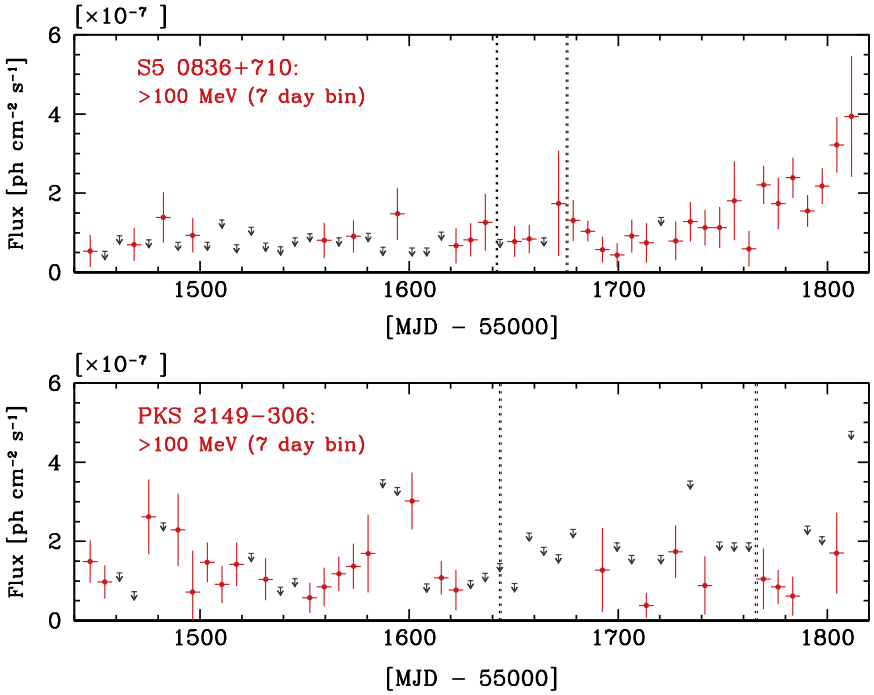

Figure 1. Gamma-ray light curves (>100 MeV) of S5 0836+710 (top panel) and PKS 2149–306 (bottom panel) as observed by *Fermi*-LAT. The vertical dotted lines mark the dates of the *NuSTAR* observations. Upper limits correspond to TS < 4 (see text).

observations. For bins with test statistic TS < 4, 95% confidence level upper limits are plotted (for the meaning of TS see Mattox et al. 1996). We fitted the 1 yr *Fermi*-LAT spectrum for each source with a power-law model, finding a best-fit photon spectral index of $\Gamma = 2.89 \pm 0.09$ (TS = 210) and $\Gamma = 2.69 \pm 0.10$ (TS = 284) for PKS 2149–306 and S5 0836+710, respectively (errors are at the 68% confidence interval for one parameter of interest). The corresponding average 1 yr fluxes are $F(>100\,\mathrm{MeV}) = (8.4 \pm 0.9) \times 10^{-8}$ photons cm^{-2} s^{-1} and $F(>100\,\mathrm{MeV}) = (5.6 \pm 0.8) \times 10^{-8}$ photons cm^{-2} s^{-1}.

In the case of S5 0836+710 we have enough statistics to extract a 1 month (2014 January 1–February 1) source spectrum centered around the second *NuSTAR* observation. The fitting result yielded $\Gamma = 2.7 \pm 0.2$ (TS = 46) with an average flux above 100 MeV of $(8.7 \pm 1.9) \times 10^{-8}$ photons cm^{-2} s^{-1}. From Figure 1 it is also apparent that a couple of months later the source became much more active in the *Fermi*-LAT band.

2.5. X-Ray Spectral Analysis

For all observations of both sources simultaneous fits of the XRT and *NuSTAR* spectra were performed using the XSPEC package. In both cases a broken power-law model with an absorption hydrogen-equivalent column density fixed to the Galactic value was adopted ($N_{\rm H} = 1.6 \times 10^{20}$ cm^{-2} and $N_{\rm H} = 2.8 \times 10^{20}$ cm^{-2} for PKS 2149–306 and S5 0836+710, respectively; Kalberla et al. 2005). To allow for the cross-calibration uncertainties between the three telescopes (two *NuSTAR* and one *Swift*), a multiplicative constant factor has been included, kept equal to 1 for the FPMA spectra and free to vary for the FPMB and XRT spectra. In the case of FPMB the difference is in the range of 2%–4%, while for XRT it is somewhat larger but always less than 10%. This is consistent with the values usually found for other sources. We find that this model provides a good description of the observed spectra in the 0.3–79 keV energy band. The results of the spectral fits are in Table 3, while Figure 2 shows an example of the XRT and *NuSTAR* spectra, together with the best-fit model for the observation of PKS 2149–306 on 2014 April 18. To test the robustness of the spectral curvature, we estimated the instrumental cross-calibration factors by fitting the data in a common energy band (3–9 keV), adopting a power-law model. We found fully consistent best-fit values of the cross-calibration factors. We then verified that the broken power-law best-fit spectral results were unchanged using these values. Besides using a broken power-law model, we tried a simpler power-law model, but this did not provide a good fit to the data for either source. In fact, in all cases the reduced χ_r^2 was larger than 1.1–1.2 with more than 900 degrees of freedom. The *F*-test shows that the improvement of these values obtained with the broken power-law model is significant, with a probability smaller than 10^{-30} in three cases and smaller than 10^{-11} in one case. Moreover, when using the power-law model, the constant value included to take into account the cross-calibration uncertainties was too large or too low (e.g., 20%–30% difference) with respect to the values usually found, another indication that the single power-law model is not correct.

In Table 3 we also provide the fluxes in the two bands 2–10 keV and 10–40 keV for the four observations. Both sources have varied between the two observations, spanning a timescale of 1 month for S5 0836+710 and of 4 months for PKS 2149–306. No fast variability is observed during the single observations. However, while for S5 0836+710 there is an increase by a factor of ∼1.5 over the full 0.3–79 keV band, with a hint of lower variability below ∼1 keV, for PKS 2149–306 a variability of ∼30% is present essentially only above 10 keV. To better show this, we plot all XRT and *NuSTAR* spectra in Figure 3.

Table 3
Parameters of the X-ray Spectral Analysis for the Simultaneous Fit of the *NuSTAR* and *Swift*/XRT Data

PKS 2149–306						
Date	Γ_1	Γ_2	Break (keV)	$F_{2-10\,\mathrm{kev}}$ (erg cm^{-2} s^{-1})	$F_{10-40\,\mathrm{kev}}$ (erg cm^{-2} s^{-1})	χ^2/dof
2013 Dec 17	$0.94^{+0.07}_{-0.08}$	$1.35^{+0.02}_{-0.01}$	$2.61^{+0.67}_{-0.46}$	2.2×10^{-11}	5.0×10^{-11}	1095.8/1108
2014 Apr 18	$0.97^{+0.07}_{-0.09}$	$1.46^{+0.02}_{-0.02}$	$3.25^{+1.36}_{-0.63}$	1.9×10^{-11}	3.7×10^{-11}	936.2/952
S5 0836+710						
Date	Γ_1	Γ_2	Break (keV)	$F_{2-10\,\mathrm{kev}}$ (erg cm^{-2} s^{-1})	$F_{10-40\,\mathrm{kev}}$ (erg cm^{-2} s^{-1})	χ^2/dof
2013 Dec 15	$1.03^{+0.20}_{-0.32}$	$1.66^{+0.02}_{-0.02}$	$1.73^{+1.27}_{-0.48}$	1.6×10^{-11}	2.3×10^{-11}	642.6/611
2014 Jan 18	$1.18^{+0.08}_{-0.10}$	$1.66^{+0.02}_{-0.01}$	$2.84^{+1.03}_{-0.62}$	2.5×10^{-11}	3.6×10^{-11}	896.4/892

Note. The errors are at the 90% level of confidence for one parameter of interest. Fluxes are corrected for the Galactic absorption.

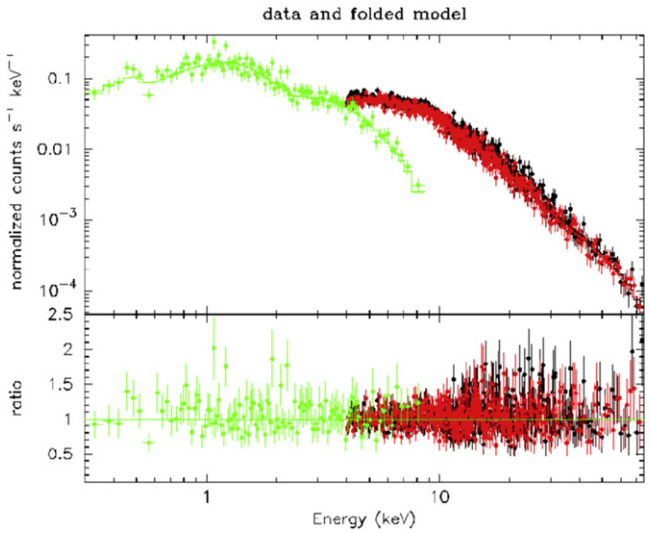

Figure 2. X-ray spectrum of PKS 2149–306 as observed by *Swift*/XRT and *NuSTAR* on 2014 April 18, together with the broken power-law best-fit model. *NuSTAR* data are filled circles and triangles (black and red, in the electronic version), while *Swift*/XRT data are open squares (green in the electronic version).

3. OVERALL SED

Figure 4 shows the X-ray data of both sources and compares them with archival observations. For S5 0836+710 the two observations correspond to different flux levels and slightly different spectra. The XRT spectrum smoothly joins the *NuSTAR* data points in both observations. The two data sets differ mainly around 10 keV, by a factor of ∼1.6, with fewer variations at both ends of the observed X-ray band. On the contrary, for PKS 2149–306 the variability amplitude monotonically increases at higher frequencies, while the two spectra are very similar in the soft X-ray band. The archival data (orange symbols) indicate that both sources (but especially S5 0836+710) can vary in X-rays by about an order of magnitude. Note also the much softer archival spectrum of PKS 2149–306 by *XMM* (and by *INTEGRAL*).

Figure 5 shows the overall SED of the two sources. Both of them show, besides the typical double-peak SED of blazars, a third narrow peak in the IR–UV band, which we identify as thermal emission from the accretion disk. Fitting it with a standard Shakura & Sunyaev (1973) disk, we find both the disk luminosity L_d and the black hole mass M (as listed in Tables 4 and 5; see Calderone et al. 2013 for a full discussion of this method). For a given efficiency η (defined through $L_\mathrm{d} = \eta \dot{M} c^2$), and when the peak of the disk emission is visible, this method returns a value of the black hole mass with a relatively small uncertainty (factor of ∼1.5), better than the virial method (factor of 3–4; Vestergaard & Peterson 2006; Park et al. 2012). Adopting $\eta = 0.08$, we find a black hole mass of $5 \times 10^9 M_\odot$ for S5 0836+710 and $3.5 \times 10^9 M_\odot$ for PKS 2149–306.[20] These values differ slightly from what we reported previously using the same method (in Ghisellini et al. 2010a, hereafter GG10). This is due to the better coverage of the IR part of the spectrum now available from *WISE* and REM. With these values of the black hole mass, the disks of both sources emit at ∼20%–30% of the Eddington luminosity. The blazar S5 0836+710 has also been monitored for reverberation mapping by Kaspi et al. (2007). Using the observed lag between the continuum, the C IV FWHM, and Equation (5) of Kaspi et al. (2000), they obtained a black hole mass $M = 2.6 \times 10^9 M_\odot$. Instead, using the UV luminosity, the C iv FWHM, and Equation (7) of Vestergaard & Peterson (2006), they derive $M = 1.8 \times 10^{10} M_\odot$.

As discussed also in GG10, these sources are *weak* in the γ-ray band. This is due to two effects. The first is a k-correction effect: for increasing redshifts, the observed hard X-ray spectrum is closer to the high-energy peak and thus brighter. The second effect is due to the intrinsic shift of the high-energy peak frequency as the bolometric nonthermal luminosity is increased. This implies that the most powerful jetted sources can be better found in hard X-ray surveys rather than in γ-ray surveys (GG10). For S5 0836+710 *Fermi*-LAT detected the source in 1-month integration times around the second *NuSTAR* observation (filled red points with black circles), while PKS 2149–306 is detected using 1 yr integration times (from 2013 June 1 to 2014 June 1). Both γ-ray spectra are steep, as usual for powerful FSRQs (see, e.g., Nolan et al. 2012). The fact that the synchrotron far-mm-IR spectrum is steep is consistent with the assumption that both the low- and high-energy nonthermal peaks of the SED are produced by the same population of electrons.

[20] The values of the black hole masses are somewhat dependent on η: the larger η, the greater the black hole mass. For instance, adopting $\eta = 0.06$ (0.15), we would obtain $M = 3 \times 10^9 M_\odot$ ($6 \times 10^9 M_\odot$) for S5 0836+710.

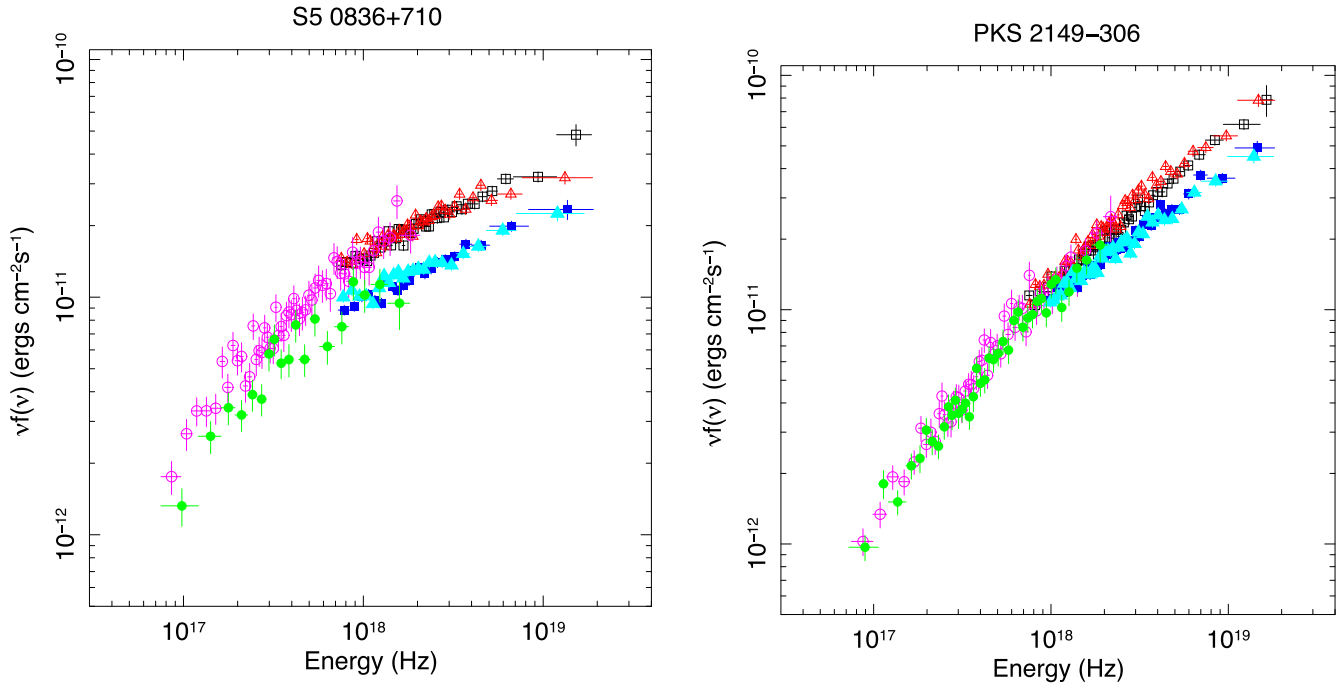

Figure 3. X-ray SED of S5 0836+710 (left panel) and of PKS 2149–306 (right panel) as observed by *Swift*/XRT and *NuSTAR* on four different dates (see the text). XRT data points are filled/open circles (green and purple in the electronic version), *NuSTAR*/FPMA data points are filled/open squares (red and blue in the electronic version), and *NuSTAR*/FPMB data points are filled/open triangles (black and magenta in the electronic version).

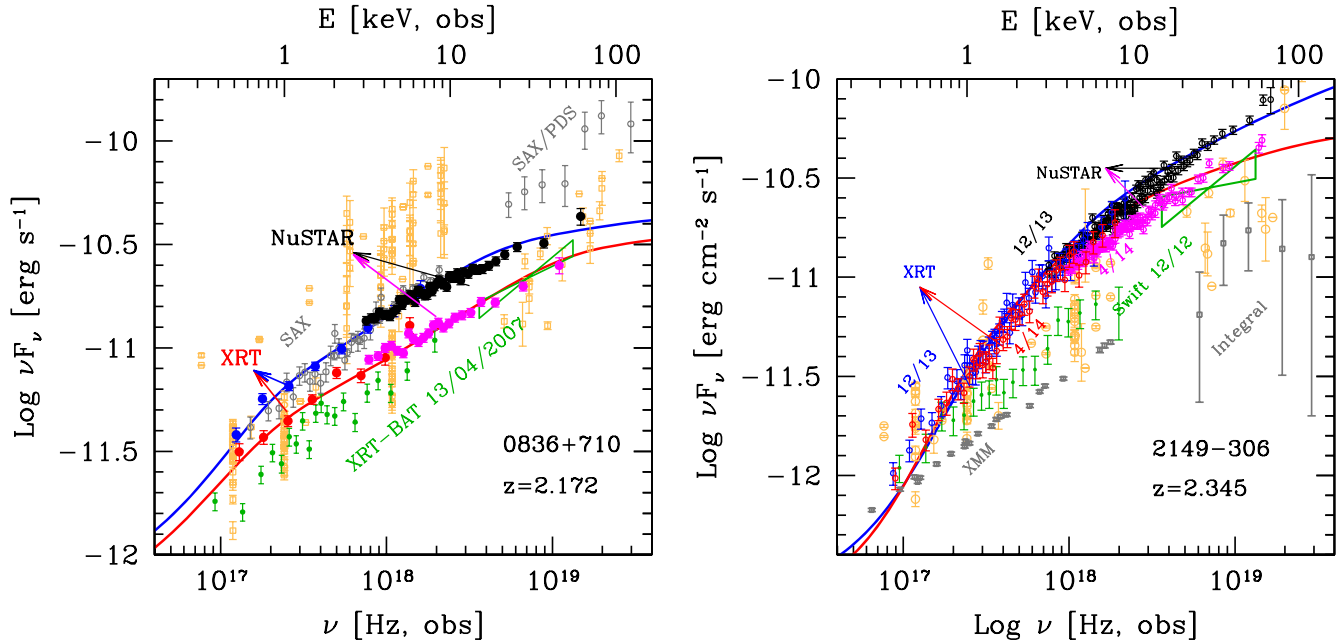

Figure 4. X-ray SED of S5 0836+710 (left panel) and PKS 2149–306 (right panel) as observed by *Swift*/XRT and *NuSTAR*, compared with previous observations by *Swift* (green dots), *INTEGRAL*, *XMM*, and *BeppoSAX* (gray), and other archival observations (orange). Our XRT and *NuSTAR* data points for the two observing periods are labeled. The solid lines refer to the model used to explain the overall SED, as shown in Figure 5.

We applied a one-zone leptonic model, fully described in Ghisellini & Tavecchio (2009), to interpret the SED of the two sources and to explore the variability that both sources experienced between the two *Swift*+*NuSTAR* observations. In brief, the model assumes that the emitting source is a homogeneous sphere located at a distance $R_{\rm diss}$ from the black hole, in a conical jet of semi-aperture angle $\phi = 0.1$ rad. The broad-line region (BLR) is assumed to be a spherical shell of radius $R_{\rm BLR} = 10^{17} L_{\rm d,45}^{1/2}$ cm, and the size of the IR torus is assumed to be $R_{\rm torus} = 2 \times 10^{18} L_{\rm d,45}^{1/2}$ cm (here $L_{\rm d,45}$ is the disk luminosity in units of 10^{45} erg s^{-1}). The source is assumed to move with a bulk Lorentz factor Γ in a direction making an angle $\theta_{\rm v}$ with the line of sight. The magnetic field B (as measured in the comoving frame) depends on the distance from the black hole and the bulk Lorentz factor, to yield a constant Poynting flux $P_{\rm B} \propto B^2 R_{\rm diss}^2 \Gamma^2$.

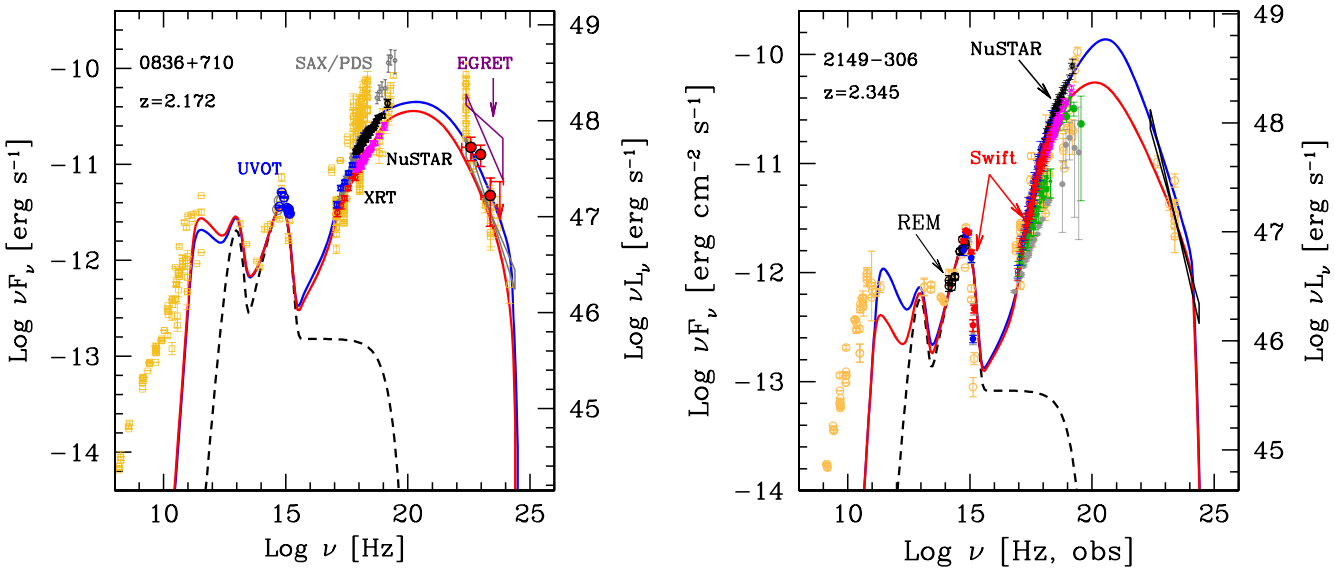

Figure 5. Overall SED of S5 0836+710 (left panel) and of PKS 2149–306 (right panel). The indicated REM, UVOT, XRT, and *NuSTAR* data are simultaneous. For S5 0836+710, the *Fermi*-LAT γ-ray data (red points encircled by black circles) are time integrated over a month (2014 January 1–February 1), centered on the second *NuSTAR* observation, while the bow tie represents the result of the 1 yr integration (2013 June 1–2014 June 1). For PKS 2149–306, the *Fermi*-LAT data (bow tie) are the result of the 1 yr integration (2013 June 1–2014 June 1). The solid lines refer to the one-zone leptonic model discussed in the text. The dashed black line is the contribution of the accretion disk, the IR torus, and the X-ray corona. We also show archival data (open circles, orange in the electronic version).

Table 4
Input Parameters Used to Model the SED

Name (1)	M (2)	Γ (3)	θ_v (4)	R_{diss} (5)	R (6)	R_{BLR} (7)	P'_i (8)	B (9)	γ_b (10)	γ_{max} (11)	s_1 (12)	s_2 (13)	γ_c
0836+710 H	5e9	16	3	1950	195	1500	0.11	1.11	250	5e3	1.7	3.2	5.7
0836+710 L	5e9	16	3	2100	210	1500	0.09	1.04	190	4e3	1.6	3.2	9.8
0836+710 GG10	3e9	14	3	540	54	1500	0.22	3.28	90	2e3	−1	3.6	2.1
2149–306 H	3.5e9	14	3	1365	137	1212	0.2	1.05	75	4e3	0.5	3.3	2.9
2149–306 L	3.5e9	14	3	1365	137	1212	0.1	1.05	50	4e3	1	3.0	2.9
2149–306 GG10	5e9	15	3	1200	120	1224	0.18	1.12	60	3e3	0	3.3	1

Note. "L" and "H" stand for low and high state, respectively; GG10 stands for Ghisellini et al. (2010a), where the two sources were also studied. Column [1]: source name and state/observation; column [2]: black hole mass in solar mass units; column [3]: bulk Lorentz factor; column [4]: viewing angle (degrees); column [5]: distance of the blob from the black hole in units of 10^{15} cm; column [6]: source size in units of 10^{15} cm; column [7]: size of the broad-line region in units of 10^{15} cm; column [8]: power injected in the blob calculated in the comoving frame, in units of 10^{45} erg s^{-1}; column [9]: magnetic field in G; column [10] and [11]: minimum and maximum random Lorentz factors of the injected electrons; column [12] and [13]: slopes of the injected electron distribution [$Q(\gamma)$] below and above γ_b; column [13]: value of the minimum random Lorentz factor of the electrons cooling in R/c. The spectral shape of the corona is assumed to be $\propto \nu^{-1}\exp(-h\nu/150\,\mathrm{keV})$.

Table 5
Accretion and Jet Powers

Name (1)	log L_d (2)	L_d/L_{Edd} (3)	log P_r (4)	log P_B (5)	log P_e (6)	log P_p (7)
0836+710 H	47.4	0.3	46.8	46.7	45.9	48.6
0836+710 L	47.4	0.3	46.7	46.7	45.9	48.5
0836+710 GG10	47.4	0.5	46.6	46.4	45.5	48.0
2149–306 H	47.2	0.3	47.1	46.2	45.7	48.3
2149–306 L	47.2	0.3	46.7	46.2	45.6	48.3
2149–306 GG10	47.2	0.2	46.6	46.2	45.3	48.0

Note. Column [1]: source name and state/observation; column [2]: logarithm of the accretion disk luminosity (units are erg s^{-1}); column [3]: accretion disk luminosity in Eddington units; column [4]–[7]: logarithm of the jet power in the form of radiation (P_r), poynting flux (P_B), bulk motion of electrons (P_e), and protons (P_p) (assuming one cold proton per emitting electron). Units are erg s^{-1}. These values refer to one jet only.

The energy distribution of the emitting particles is found through the continuity equation, accounting for continuous injection, radiative cooling, and electron-positron pair production. Electrons (with random Lorentz factors $1 < \gamma < \gamma_{max}$) are assumed to be injected with a total power P'_i (in the comoving frame) throughout the source with a broken power-law distribution, $\propto \gamma^{-s_1}$ and $\propto \gamma^{-s_2}$ below and above γ_b, respectively. The radiative processes are SSC and EC with both photons from the BLR and the torus. We also consider the presence of an X-ray corona, emitting 30% of L_d with a spectrum $F_\nu \propto \nu^{-1}\exp(-h\nu/150\ \mathrm{keV})$.

Owing to the compactness of the source, required to account for the fast variability, the synchrotron emission is self-absorbed at radio frequencies, up to hundreds of GHz (observer frame). Therefore, these models cannot reproduce the radio data.

Figure 5 shows the models corresponding to the two states of each source, and Table 4 lists the model parameters. It also

reports the parameters used in GG10 to fit another data set. To model the two observed states, we changed a minimum number of parameters. Both sources have $R_{\rm torus} > R_{\rm diss} > R_{\rm BLR}$. This choice is preferred (with respect to $R_{\rm diss}$ within the BLR) because of the small value of the high-energy peak, requiring seed photons of frequency smaller than the hydrogen Lyα -photons (which dominate the BLR emission). In this respect, *NuSTAR* is crucial because the hardness of its spectrum, together with the extrapolation from the γ-ray energies, greatly helps in pinpointing the peak frequency of the high-energy hump. This is the major difference with respect to the parameters reported by GG10 for S5 0836+710, which assumed $R_{\rm diss} < R_{\rm BLR}$.

The observed variability of S5 0836+710 is ascribed to a small difference in the position of the emitting region, in turn implying a small change in the magnetic field. Furthermore, the injected power changes by 10%, and the break energy of the injected electron distribution changes by 20%.

For PKS 2149–306 the variability can be explained by changing the injected power by a factor of 2, as well as by a 50% change in the break energy of the injected electron distribution.

Comparing these changes with the distribution of the parameters in many *Fermi*-LAT blazars (as listed, e.g., in Ghisellini et al. 2010b), we conclude that the changes required to explain the observed (factor of ∼1.5) variability are very small.

4. DISCUSSION AND CONCLUSIONS

The simultaneous observations of *NuSTAR* and *Swift*/XRT revealed that the X-ray spectra from ∼0.3 to 60 keV of both sources are well described by a broken power-law model. Both indices are very hard, with no requirement of absorption in excess of the Galactic one. This broken power-law behavior is well reproduced by the model as a result of a combination of two effects. First, the electron energy distribution, below the cooling energy $\gamma_{\rm c}$, retains the slope of the injected electrons (i.e., γ^{-s_1}), which is very hard (see Table 4). Second, what we observe as low-energy X-ray emission at the frequency ν_x is seen, in the comoving frame, as ultraviolet emission (i.e., $\nu'_x = \nu_x(1+z)/\delta$), produced by the scattering between low-energy electrons and seed photons with frequencies smaller than ν'_x. In both sources, the main contributions to the seed photons come from the IR torus, the BLR, and the disk. All these components have a corresponding radiation energy density peaking at some frequency, which is seen between the optical and the UV in the comoving frame of the jet. Inverse Compton scattered photons at, for example, $\nu' \sim 10^{15}$ Hz can be produced using seed photons of frequencies smaller than 10^{15} Hz, which do not correspond to the full energy density of the seed photons. Scattered photons of higher energies, instead, can use the entire seed photon distribution. In other words, there is a paucity of seed photons at low energies, making the inverse Compton spectrum harder below a few keV. What is observed in the two blazars studied here can then be regarded as a proof of the "EC" process, where the major contribution to the seed photons comes from radiation produced externally to the jet. Furthermore, the spectrum between 0.3 and 60 keV is smooth, indicating the absence of other emitting components.

Both blazars show variability, but not extreme variability. This agrees with a relatively large source size and a correspondingly relatively large distance from the black hole. The observed light-crossing time predicted by our model is $t_{\rm var}^{\rm obs} \equiv (R/c)(1+z)/\delta$, corresponding to ∼13 days for S5 0836+710 and ∼10 days for PKS 2149–306. This agrees with no variability observed within a single-epoch observation and is consistent with the emission site being between the BLR and the torus ($R_{\rm BLR} < R_{\rm diss} < R_{\rm torus}$). We note that, contrary to what we have observed, significant variability on shorter timescales has been reported for S5 0836+710 by Akyuz et al. (2013). In the framework of our modeling this is explained by assuming that the component dominating the emission at a given time is not always located in the same place along the jet. Sometimes it can be at a position closer to the black hole and be more compact, giving rise to variability on shorter timescales and to a slightly different SED.

We have shown that the observed moderate variability can be produced by a rather small change in the injected power, break energy of the electron distribution, and the location of the emitting region. The largest change is needed for PKS 2149–306, requiring a factor of 2 change in the injected power.

The *NuSTAR* data at high energies, coupled with the γ-ray data, allow us to determine where the high-energy hump of the SED peaks. This is at ∼1 MeV (observed, thus ∼3 MeV, rest frame) for both sources. As already mentioned, this helps to determine the location of the emitting region, making us prefer an emitting region located between the BLR and the torus. We stress that this may not necessarily always be the case since the emitting site can change, and sometimes it can be within the BLR. For a given electron distribution, the high-frequency peak would shift to higher values, in this case. The data of S5 0836+710 have been analyzed also by Paliya (2015), who fit the data using the same single-zone leptonic emission model. We find consistent results, but our black hole mass is slightly larger, and our emitting region is just outside the BLR, while in Paliya (2015) it is inside. We find that while the parameters of Paliya (2015) indeed satisfactorily fit the overall SED and the average *NuSTAR* spectrum, our fit accounts for the two states of the source in a better way, and in particular the two sets of *Swift*/XRT+*NuSTAR* data.

Both blazars have a black hole with mass exceeding $10^9 M_\odot$ and accretion disks emitting at about one-third of the Eddington rate. The power that the jet expends for producing the radiation we see ($P_{\rm r}$ in Table 5) is of the same order as $L_{\rm d}$ (note that the listed values of $P_{\rm r}$ refer to one jet only and should be doubled). $P_{\rm r}$ is a *lower limit* of the true jet power $P_{\rm jet}$. An estimate of $P_{\rm jet}$ can be derived assuming, following Nemmen et al. (2012), that $P_{\rm jet} \sim 10 P_{\rm r}$. Another estimate can be found assuming that there is one proton for each emitting electron (this is the quantity $P_{\rm p}$ in Table 5). Either way, we are forced to conclude that the jet power exceeds the luminosity of the accretion disk, thus suggesting that the jet is powered not only by accretion but also by the rotational energy of a spinning black hole, as found by Ghisellini et al. (2014) for a large sample of blazars.

Finally, given the very hard spectra detected by *NuSTAR* - and their high-energy peak at ∼1–10 MeV, one can wonder whether powerful blazars can significantly contribute to the X-ray background above its ∼30 keV peak. While a complete study of this issue is still missing, there are preliminary results by Draper & Ballantyne (2009), Giommi (2011), and Comastri & Gilli (2011) suggesting that blazars can contribute at the 10% level at ∼100 keV, before becoming the dominant

contributors to the γ-ray background (Abdo et al. 2010; Ajello et al. 2015).

We acknowledge financial support from the ASI-INAF grant I/037/12/0. This work was supported under NASA Contract No. NNG08FD60C and made use of data from the *NuSTAR* mission, a project led by the California Institute of Technology, managed by the Jet Propulsion Laboratory, and funded by NASA. We thank the *NuSTAR* Operations, Software and Calibration teams for support with the execution and analysis of these observations. We also thank the *Swift* team for quickly approving and executing the requested ToO observations. This research has made use of the *NuSTAR* Data Analysis Software (NuSTARDAS) jointly developed by the ASI Science Data Center (ASDC, Italy) and the California Institute of Technology (Caltech, USA). The *Fermi*-LAT Collaboration acknowledges generous ongoing support from a number of agencies and institutes that have supported both the development and the operation of the LAT, as well as scientific data analysis. These include the National Aeronautics and Space Administration and the Department of Energy in the United States; the Commissariat à l'Energie Atomique and the Centre National de la Recherche Scientifique/Institut National de Physique Nucléaire et de Physique des Particules in France; the Agenzia Spaziale Italiana and the Istituto Nazionale di Fisica Nucleare in Italy; the Ministry of Education, Culture, Sports, Science and Technology (MEXT), High Energy Accelerator Research Organization (KEK), and Japan Aerospace Exploration Agency (JAXA) in Japan; and the K. A. Wallenberg Foundation, the Swedish Research Council, and the Swedish National Space Board in Sweden. Additional support for science analysis during the operations phase is gratefully acknowledged from the Istituto Nazionale di Astrofisica in Italy and the Centre National d'Études Spatiales in France. Part of this work is based on archival data, software, or online services provided by the ASI Data Center (ASDC).

REFERENCES

Abdo, A. A., Ackermann, M., Ajello, M., et al. 2010, ApJ, 720, 435
Acero, F., Ackermann, M., Ajello, M., et al. 2015, ApJS, 218, 23
Ajello, M., Costamante, L., Sambruna, R. M., et al. 2009, ApJ, 699, 603
Ajello, M., Gasparrini, D., Sanchez-Conde, M., et al. 2015, ApJL, 800, L27
Ajello, M., Romani, R. W., Gasparrini, D., et al. 2014, ApJ, 780, 73
Akyuz, A., Thompson, D. J., Donato, D., et al. 2013, A&A, 556, 71
Atwood, W. B., Abdo, A. A., Ackermann, M., et al. 2009, ApJ, 697, 1071
Baars, J. W. M., Genzel, R., Paulini-Toth, I. I. K., & Witzel, A. 1977, A&A, 61, 99
Beckmann, V., Gehrels, N., Shrader, C. R., & Soldi, S. 2006, ApJ, 638, 642
Bianchin, V., Foschini, L., Ghisellini, G., et al. 2009, A&A, 496, 423
Bock, D. C.-J., Bolatto, A. D., Hawkins, D. W., et al. 2006, Proc. SPIE, 6267, 13
Burrows, D., Hill, J., Nousek, J., et al. 2005, SSRv, 120, 165
Calderone, G., Ghisellini, G., Colpi, M., & Dotti, M. 2013, MNRAS, 431, 210
Cash, W. 1979, ApJ, 228, 939
Comastri, A., & Gilli, R. 2011, in The Second Ferrara Workshop on X-ray Astrophysics up to 511 keV, 16
Conconi, P., Cunniffe, R., D'Alessio, F., et al. 2004, Proc. SPIE, 5492, 1602
Covino, S., Stefanon, M., Sciuto, G., et al. 2004, Proc. SPIE, 5492, 1613
Cusumano, G., La Parola, V., Segreto, A., et al. 2010, A&A, 524, 64
Draper, A. R., & Ballantyne, D. R. 2009, ApJ, 707, 778
Elvis, M., Fiore, F., Siemiginowska, A., et al. 2000, ApJ, 543, 545
Fitzpatrick, E. L., & Massa, D. 2009, ApJ, 699, 1209
Frey, S., Fogasy, J. O., Paragi, Z., & Gurvitis, L. I. 2013, MNRAS, 431, 1314
Fruscione, A., McDowell, J. C., Allen, G. E., et al. 2006, Proc. SPIE, 6270, 62701V
Gehrels, N., Chincarini, G., Giommi, P., et al. 2004, ApJ, 611, 1005
Ghisellini, G., Della Ceca, R., Volonteri, M., et al. 2010a, MNRAS, 405, 387 (GG10)
Ghisellini, G., Haardt, F., Della Ceca, R., Volonteri, M., & Sbarrato, T. 2013, MNRAS, 432, 2818
Ghisellini, G., & Tavecchio, F. 2009, MNRAS, 397, 985
Ghisellini, G., Tagliaferri, G., Foschini, L., et al. 2011, MNRAS, 411, 901
Ghisellini, G., Tavecchio, F., Foschini, L., et al. 2010b, MNRAS, 402, 497
Ghisellini, G., Tavecchio, F., Maraschi, L., Celotti, A., & Sbarrato, T. 2014, Natur, 515, 376
Giommi, P. 2011, in The Second Ferrara Workshop on X-ray Astrophysics up to 511 keV, 25
Giommi, P., Padovani, P., & Polenta, G. 2013, MNRAS, 431, 1914
Giommi, P., Padovani, P., Polenta, G., et al. 2012, MNRAS, 420, 2899
Greiner, J., Bornemann, W., Clemens, C., et al. 2008, PASP, 120, 405
Harrison, F. A., Craig, W. W., Christensen, F. E., et al. 2013, ApJ, 770, 103
Hartman, R. C., Bertsch, D. L., Bloom, D. L., et al. 1999, ApJS, 123, 79
Kalberla, P. M. W., Burton, W. B., Hartmann, D., et al. 2005, A&A, 440, 775
Kaspi, S., Brandt, W. N., Maoz, D., et al. 2007, ApJ, 659, 997
Kaspi, S., Smith, P. S., Netzer, H., et al. 2000, ApJ, 533, 631
Krühler, T., Küpcü, Y., Greiner, J., et al. 2008, ApJ, 685, 376
Mattox, J. R., Bertsch, D. L., Chiang, J., et al. 1996, ApJ, 461, 396
Molinari, E., Covino, S., Crimi, G., et al. 2014, Proc. SPIE, 9147, 260
Nemmen, R. S., Georganopoulos, M., Guiriec, S., et al. 2012, Sci, 338, 1445
Nolan, P. L., Abdo, A. A., Ackermann, M., et al. 2012, ApJS, 199, 31
Paliya, V. S. 2015, ApJ, 804, 74
Park, D., Woo, J. H., Treu, T., et al. 2012, ApJ, 747, 30
Poole, T. S., Breeveld, A. A., Page, M. J., et al. 2008, MNRAS, 383, 627
Richards, J. L., Max-Moerbeck, W., Pavlidou, V., et al. 2011, ApJS, 194, 29
Romani, R. W. 2006, AJ, 132, 1959
Romani, R. W., Sowards-Emmerd, D., Greenhill, L., & Michelson, P. 2004, ApJL, 610, L9
Roming, P. W. A., Kennedy, T. E., Mason, K. O., et al. 2005, SSRv, 120, 95
Sambruna, R. M., Tavecchio, F., Ghisellini, G., et al. 2007, ApJ, 669, 884
Sault, R. J., Teuben, P. J., & Wright, M. C. H. 1995, ASP Conf. Ser. 77, Astronomical Data Analysis Software and Systems IV, ed. R. A. Shaw, H. E. Payne & J. J. E. Hayes (San Francisco, CA: ASP), 433
Sbarrato, T., Ghisellini, G., Nardini, M., et al. 2012, MNRAS, 426, L91
Sbarrato, T., Ghisellini, G., Nardini, M., et al. 2013, MNRAS, 433, 2182
Schlafly, E. F., & Finkbeiner, D. P. 2011, ApJ, 737, 103
Schlegel, D.-J., Finkbeiner, D. P., & Davis, M. 1998, ApJ, 500, 525
Shakura, N. I., & Sunyaev, R. A. 1973, A&A, 24, 337
Shaw, M., Romani, R. W., Cotter, G., et al. 2013, ApJ, 764, 135
Sikora, M., Stawarz, L., & Lasota, J. P. 2007, ApJ, 658, 815
Skrutskie, M. F., Cutri, R. M., Stiening, R., et al. 2006, AJ, 131, 1163
Tavecchio, F., Maraschi, L., Ghisellini, G., et al. 2000, ApJ, 543, 535
Thorne, K. S. 1974, ApJ, 191, 507
Tody, D. 1993, in ASP Conf. Ser., 52, Astronomical Data Analysis Software and Systems II, ed. R. J. Hanisch, R. J. V. Brissenden & J. Barnes (San Francisco, CA: ASP), 173
Vestergaard, M., & Peterson, B. M. 2006, ApJ, 641, 689
Volonteri, M., Haardt, F., Ghisellini, G., & Della Ceca, R. 2011, MNRAS, 416, 216
Willott, C. J., Albert, L., Arzoumanian, D., et al. 2010, AJ, 140, 546
Wilson, A. S., & Colbert, E. J. M. 1995, ApJ, 438, 62
Worsley, M. A., Fabian, A. C., Celotti, A., & Iwasawa, K. 2004, MNRAS, 350, L67
Wright, E. L., Eisenhardt, P. R. M., Mainzer, A. K., et al. 2010, AJ, 140, 1868
Wu, J., Brandt, W. N., Miller, B. P., et al. 2013, ApJ, 763, 109
Zerbi, F., Chincarini, G., Ghisellini, G., et al. 2004, Proc. SPIE, 5492, 1590